

Landfast ice thickness in the Canadian Arctic Archipelago from Observations and Models

Stephen. E. L. Howell¹, Frédéric Laliberté¹, Ron Kwok², Chris Derksen¹ and Joshua King¹

¹Climate Research Division, Environment Canada, Toronto, Canada

²Jet Propulsion Laboratory, California Institute of Technology, Pasadena, California, USA

Abstract

Observed and modelled landfast ice thickness variability and trends spanning more than five decades within the Canadian Arctic Archipelago (CAA) are summarized. The observed sites (Cambridge Bay, Resolute, Eureka and Alert) represent some of the Arctic's longest records of landfast ice thickness. Observed end-of-winter (maximum) trends of landfast ice thickness (1957-2014) were statistically significant at Cambridge Bay (-4.31 ± 1.4 cm decade⁻¹), Eureka (-4.65 ± 1.7 cm decade⁻¹) and Alert (-4.44 ± 1.6 cm decade⁻¹) but not at Resolute. Over the 50+ year record, the ice thinned by ~0.24-0.26 m at Cambridge Bay, Eureka and Alert with essentially negligible change at Resolute. Although statistically significant warming in spring and fall was present at all sites, only low correlations between temperature and maximum ice thickness were present; snow depth was found to be more strongly associated with the negative ice thickness trends. Comparison with multi-model simulations from Coupled Model Intercomparison project phase 5 (CMIP5), Ocean Reanalysis Intercomparison (ORA-IP) and Pan-Arctic Ice-Ocean Modeling and Assimilation System (PIOMAS) show that although a subset of current generation models have a 'reasonable' climatological representation of landfast ice thickness and distribution within the CAA, trends are unrealistic and far exceed observations by up to two orders of magnitude. ORA-IP models were found to have positive correlations between temperature and ice thickness over the CAA, a feature that is inconsistent with both observations and coupled models from CMIP5.

24 **1. Introduction**

25 The World Meteorological Organization (WMO, 1970) defines landfast sea ice as “sea ice
26 which remains fast along the coast, where it is attached to the shore, to an ice wall, to an ice front,
27 or over shoals, or between grounded icebergs.” In the Arctic, this ice typically extends to the 20-
28 30 m isobaths [Mahoney *et al.*, 2007; Mahoney *et al.*, 2014]. It melts each summer and reforms in
29 the fall but there are regions along the northern coast of the Canadian Arctic Archipelago (CAA)
30 where multi-year landfast ice (also termed an “ice plug”) is present. The two most prominent
31 regions of multi-year landfast sea ice in the CAA are located in Nansen Sound and Sverdrup
32 Channel [Serson, 1972; Serson, 1974] (Figure 1). It has been documented that ice remained intact
33 from 1963-1998 in Nansen Sound and from 1978-1998 in Sverdrup Channel [Jeffers *et al.*, 2001;
34 Melling, 2002; Alt *et al.*, 2006]. The extreme warm year of 1998 disintegrated the ice in both
35 regions and their survival during the summer melt season in recent years has occurred less
36 frequently [Alt *et al.*, 2006]. Over the entire Arctic, landfast ice extent is declining at 7% decade⁻¹
37 since the mid-1970s [Yu *et al.*, 2013]

38 Records of landfast ice thickness provide annual measures of ice growth that can also
39 almost entirely be attributed to atmospheric forcing with negligible deep ocean influence on local
40 ice formation. While the key forcings on landfast ice and offshore ice are different, the seasonal
41 behavior of landfast ice can nevertheless provide useful information for understanding the
42 interannual variability of ice thickness in both regimes. Presently, there is no pan-Arctic network
43 for monitoring changes in landfast ice but available measurements suggest thinning in recent years.
44 Thickness measurements near Hopen, Svalbard revealed thinning of landfast ice in the Barents
45 Sea region by 11 cm decade⁻¹ between 1966 and 2007 [Gerland *et al.*, 2008]. From a composite
46 time series of landfast ice thickness from 15 stations along the Siberian coast, Polyakov *et al.*

47 [2010] estimate an average rate of thinning of 3.3 cm decade⁻¹ between the mid-1960s and early
48 2000s. Relatively recent observations by *Mahoney et al.* [2007] and *Druckenmiller et al.* [2009]
49 found longer ice-free seasons and thinner landfast ice compared to earlier records.

50 At four sites in the CAA, *Brown and Cote* [1992] (hereinafter, BC92) provided the first
51 examination of the interannual variability of end-of-winter (maximum) landfast ice thickness and
52 associated snow depth over the period 1957-1989. Their results highlighted the insulating role of
53 snow cover in explaining 30-60% of the variance in maximum ice thickness. Similar results were
54 also reported by *Flato and Brown* [1996] and *Gough et al.* [2004]. In the record examined by
55 BC92, no evidence for systematic thinning of landfast ice in the CAA was found. Landfast ice
56 thickness records at several of these CAA sites are now over 50 years in length, which represents
57 an addition of more than two decades of measurements since BC92 during a period that saw
58 dramatic reductions in the extent and thickness of Arctic sea ice [e.g. *Kwok and Rothrock*, 2009;
59 *Stroeve et al.*, 2012].

60 The sparse network of long term observations of snow and ice thickness in the Arctic
61 (clearly exhibited by only four ongoing measurements sites operated by Environment Canada in
62 the CAA) has made the use of models imperative to provide a broader regional scale perspective
63 of sea ice trends in a warming climate. Given the coarse spatial resolution of global climate models,
64 previous studies focusing on the CAA have relied on either a one-dimensional thermodynamic
65 dynamic model [*Flato and Brown*, 1996; *Dumas et al.*, 2006] or a regional three-dimensional ice-
66 ocean coupled model [e.g. *Sou and Flato*, 2009]. Specifically, *Dumas et al.* [2006] found projected
67 maximum ice thickness decreases of 30 cm by 2041-2060 and 50 cm by 2081-2100 and *Flato and*
68 *Sou* [2009] reported a potential 17% decrease in overall ice thickness throughout the CAA by
69 2041-2060. However, in recent years some global climate models, reanalysis products, and data

70 assimilation systems are now of sufficient spatial resolution to assess potential landfast ice
71 thickness changes within the CAA.

72 This analysis examines the trends of measured landfast ice thickness, snow depth and air
73 temperature over a 50+ year period between 1957 and 2014 and compares the results with the
74 earlier analysis by BC92. We then use this observational foundation to evaluate the
75 representativeness of landfast ice in state-of-the-art global climate models, assimilation systems
76 and re-analysis products.

77

78 **2. Data Description**

79 **2.1. Observations**

80 Landfast ice thickness and corresponding snow depth measurement have been made
81 regularly at many coastal stations throughout Canada since about 1950. These data are quality
82 controlled and archived at the Canadian Ice Service (CIS) and represent one of the few available
83 sources of continuous ice thickness measurements in the Arctic. In general, thickness
84 measurements are taken once per week, starting after freeze-up when the ice is safe to walk on and
85 continuing until breakup or when the ice becomes unsafe. Complete details of this dataset are
86 provided by Brown and Cote (1992) and the dataset is available on the CIS web site
87 (<http://www.ec.gc.ca/glaces-ice/>, see Archive followed by Ice Thickness Data). Four sites in the
88 CAA were selected for study: Alert, Eureka, Resolute, and Cambridge Bay (Figure 1). Although
89 there are other sites in the database, these sites are the only ones that span the same 55-year period
90 between 1960 and 2014. The record at Mould Bay, used in BC92, terminated in the early 1990s.
91 Together these sites cover $\sim 20^\circ$ in latitude (Figure 1) that are adjacent to an area of thick Arctic
92 sea ice that experienced the highest thinning in recent years [Kwok and Rothrock, 2009; Laxon et

93 *al.*, 2013]. Values of maximum or end-of-winter ice thickness and corresponding snow depth
94 during the ice growth season were extracted from the weekly ice and snow thickness data at the
95 selected sites. As this study is concerned with annual variability in maximum ice thickness, the
96 main period of interest extends from September to late May.

97 The other source of observed data used in this study were monthly mean air temperature
98 records at Alert, Eureka, Resolute, and Cambridge Bay for which a complete description is
99 provided by *Vincent et al.* [2012].

100

101 **2.2. Models**

102 The representation of CAA landfast sea ice thickness within the Coupled Model
103 Intercomparison project phase 5 (CMIP5) is analyzed using the -2005 Historical experiment
104 followed by the 2006-2099 Representative Concentration Pathway 8.5 (RCP85) experiment
105 [*Taylor et al.*, 2012] (Table 1). Monthly sea ice thickness (variable *sit*), sea ice concentration
106 (variable *sic*), 2 meter temperature (variable *tas*) and snow depth (variable *snd*) were used. The
107 CMIP5 data were retrieved from the British Atmospheric Data Centre database and accessed
108 through the Center for Environmental Data Analysis (www.ceda.ac.uk). Ensemble r6i1p1 and
109 r7i1p1 from model EC-EARTH were removed because of corrupted data. We obtain the multi-
110 model mean of trends at each grid point by creating the distribution of trends through a Monte-
111 Carlo simulation. We use a t-distribution for the interannual variability and build a noise model to
112 account for internal variability as in *Swart et al.* [2014] and *Laliberté et al.* [2016]. The multi-
113 model mean and its statistical significance is then obtained from the distribution. We obtain the
114 multi-model mean of Pearson correlations by first performing a Fisher transform and then apply

115 the same method as for the trends. The inverse Fisher transform is applied after obtaining the multi-
116 model mean and its significance.

117 We also investigate ice thickness values from a selection of the highest resolution models
118 [*Storto et al.*, 2011; *Forget et al.*, 2015; *Haines et al.*, 2014, *Zuo et al.*, 2015; *Masina et al.*, 2015]
119 from the Ocean Reanalysis Intercomparison (ORA-IP) [*Balsameda et al.*, 2015; *Chevallier et al.*,
120 2016] (Table 2) and from the Pan-Arctic Ice-Ocean Modeling and Assimilation System (PIOMAS)
121 [*Zhang and Rothrock*, 2003]. Supporting 2 meter temperature data was obtained from ERA-
122 Interim [*Dee et al.*, 2011].

123

124 **3. Results and Discussion: Observations**

125 **3.1. Climatology**

126 The average behavior of landfast ice at the four sites over the 50+ year record is
127 summarized in Table 3. Ice growth, approximately linear through most of the season, slows after
128 March (Figure 2). Ice thickness reaches a maximum of ~2-2.3 m by late May at all sites. Values
129 are consistent with that reported by BC92 and with recent observations of *Melling et al.* [2015]
130 and *Haas and Howell* [2015]. The standard deviations are nearly uniform (at ~0.2 m) across all
131 sites, giving a relatively low coefficient of variation (COV; a measure of relative dispersion
132 defined as the ratio of the standard deviation to the mean) of ~0.1. The thickest ice is found in
133 Eureka with a 1957-2014 mean of 2.27 m, which is likely due to climatologically lower air
134 temperatures in the fall and winter (Table 3).

135 Snow depth also appears to grow linearly through the season, peaking in May but unlike
136 ice thickness the monthly variability is high (COV ~0.4) (Figure 3). Mean October to May snow
137 depths at Resolute, Eureka and Alert range from ~18-23 cm compared to only ~8 cm at Cambridge

138 Bay (Table 3). The rapid buildup of the snow cover due to storms in the fall and early winter that
139 is evident over the Arctic Ocean multi-year ice cover [Warren *et al.*, 1999; Webster *et al.*, 2014],
140 is not seen in these snow depth records within the CAA. The linear behavior in snow depth is likely
141 maintained by continuous wind-driven redistribution and densification throughout the ice growth
142 season [BC92; Woo and Heron, 1989].

143

144 **3.2. Trends**

145 The time series of maximum ice thickness at Cambridge Bay, Resolute, Eureka and Alert
146 are illustrated in Figure 4 and summarized in Table 1. Statistically significant (95% or greater
147 confidence level) negative maximum ice thickness trends are present at Cambridge Bay (-4.31 ± 1.4
148 cm decade^{-1}), Eureka ($-4.65 \pm 1.7 \text{ cm decade}^{-1}$) and Alert ($-4.44 \pm 1.6 \text{ cm decade}^{-1}$) (Table 1). A slight
149 negative trend is present at Resolute but not statistically significant at the 95% confidence level
150 (Table 1). Over the 50+ year record, the ice thinned by $\sim 0.24\text{--}0.26$ m at Cambridge Bay, Eureka
151 and Alert with essentially negligible change at Resolute. These trends in the CAA are similar to
152 trends on the Siberian coast ($-3.3 \text{ cm decade}^{-1}$) [Polyakov *et al.*, 2010] but lower in magnitude
153 compared to the Barents Sea ($-11 \text{ cm decade}^{-1}$) [Gerland *et al.*, 2008].

154 For the shorter record (late 1950s–1989, ~ 30 years) investigated by BC92 there was a
155 negative trend at Alert ($-7.1 \text{ cm decade}^{-1}$), no evidence of a trend at Eureka, and a positive trend at
156 Resolute ($10 \text{ cm decade}^{-1}$) but only the positive trend at Resolute was statistically significant at the
157 95% or greater confidence level. Our results from the present 50+ year record suggest that the
158 negative trend at Alert is robust and the trend at Eureka is now negative and significant. The trend
159 at Resolute is now slightly negative however it is not statistically significant.

160 Typically, ice thickness reaches its maximum in late May with trends toward earlier dates
161 of maximum ice thickness present at all sites (significant at Resolute, Eureka and Alert; Table 3).
162 The significant trends are between -2.0 ± 0.1 days decade⁻¹ at Eureka to -6.2 ± 1.5 days decade⁻¹ at
163 Resolute. At Resolute, the date of maximum ice thickness is now on average more than a month
164 earlier than the early 1960's although this is not reflected in the trend in ice thickness. Freeze onset
165 at these sites is also increasing at $\sim 3-6$ days decade⁻¹ [Howell *et al.*, 2009] and demonstrates a
166 shortened growth season at Resolute, Eureka and Alert. Together, the trends of ice thickness and
167 their recorded dates suggest a systematic thinning of landfast ice at Cambridge Bay, Eureka and
168 Alert.

169

170 3.3. Ice thickness linkages with snow depth and temperature

171 The variability of landfast thickness at these Arctic sites was previously found to be largely
172 driven by interannual variations in snow depth and air temperature [BC92; Flato and Brown,
173 1996]. With the 50+ year record at the four sites, we can examine the corresponding linkages to
174 snow depth and temperature.

175 For snow depth, the only trend that is statistically significant at the 95% confidence is
176 Cambridge Bay at -0.8 ± 0.4 cm decade⁻¹ (Table 3). In contrast, BC92 found a significant positive
177 trend at Alert (4 cm decade⁻¹), a trend of low significance in Eureka, and a negative and significant
178 trend at Resolute (-3.3 cm decade⁻¹). Looking at the detrended correlations (r) between snow depth
179 and ice thickness reveals the strongest correlation at Resolute ($r=-0.71$) followed by Eureka ($r=-$
180 0.66), Alert ($r=-0.47$) and Cambridge Bay ($r=-0.31$). Figure 6 provides evidence from extreme
181 years of the role of deeper snow inhibiting ice growth compared to thinner snow, but the positive
182 trends in snow thickness are not significant at Resolute, Eureka and Alert. This may in part be due

183 to the single pointwise snow depth and ice thickness measurements made at each point in time,
184 which fail to capture spatial heterogeneity in the snow depth/ice thickness relationship.

185 With respect to observed temperature, we find significant warming trends in the spring and
186 fall at all sites over the 50+ year record (Table 3; Figure 7). Significant warming is also present at
187 all sites in the summer except Resolute and at all sites during the winter except Eureka (Table 3).
188 Warming is highest during the fall, at $\sim 0.6^{\circ}\text{C decade}^{-1}$ at all sites (Table 3). The detrended
189 correlation between temperature (winter, spring, summer and autumn) and maximum ice thickness
190 is weak at all sites. For example, the strongest detrended correlation between maximum ice
191 thickness and temperature (winter and spring) is found at Cambridge Bay during the winter and
192 spring but is only ~ 0.4 .

193 Also of interest is that the observed temperature trends over this period differ considerably
194 from the earlier period investigated in BC92, in which they reported cooling at all the sites, with a
195 significant cooling trend at Eureka. It was noted that the general cooling over their record coincided
196 with the 1946-1986 cooling trend over much of the eastern Arctic and northwest Atlantic reported
197 by *Jones et al.* [1987]. This cooling trend halted during the 1980s and the warming, seen in the
198 current and longer record, has resumed [*Jones et al.*, 1999]. Arctic land areas have experienced an
199 overall warming of about $\sim 2^{\circ}\text{C}$ since the mid-1960s, with area-wide positive temperature
200 anomalies that show systematic changes since the end of the 20th century, which continued
201 through 2014 [*Jeffries and Richter-Menge*, 2015]. Recently, warming in Canadian Arctic regions
202 was found to be greater than the pan-Arctic trend by up to $0.2^{\circ}\text{C decade}^{-1}$ [*Tivy et al.*, 2011].

203

204 **4. Results and Discussion: Models**

205 **4.1. Climatology**

206 In order to compare seasonal cycles and trends in landfast ice thickness and snow depth
207 between models and observations, we limit our comparison to models with a reasonable
208 representation of the CAA, i.e. those with an open Parry Channel (i.e. bcc-csm-1-1, bcc-csm-1-
209 1m, CNRM-CM5, ACCESS1-0, ACCESS1-3, FIO-ESM, EC-EARTH, inmcm4, MIROC5, MPI-
210 ESM-LR, MPI-ESM-MR, MRI-CGCM3, CCSM4, NorESM1-M, NorESM1-ME, GFDL-CM3,
211 GFDL-ESM2G, GFL-ESM2M, CESM1-BCG, CESM1-CAM5, CESM-WACCM). In these
212 models, sufficient spatial resolution allows us to find sample points that are almost collocated to
213 *in situ* observation locations. The sample points were determined by finding the closest ocean grid
214 point where the sea ice is packed for a good portion of the year, but not all year. Grid points with
215 this characteristic therefore share the most important feature of the landfast ice at our observations
216 locations: it is not perennial. Mathematically, we sought sample points where the sea ice
217 concentration is on average above 85% for more than one month but less than 11 months over the
218 1955-2014 period. The Eureka site is however particularly challenging for models because it lies
219 deep in a very narrow channel, which is only resolved by the MPI-ESM-MR in the CMIP5. As a
220 result, for most models, the sample point for Eureka is located on the western shore of Ellesmere
221 Island. This is a consequence of using samples as some models either do not resolve some of the
222 channels in the CAA or have too perennial packed ice cover (e.g. CESM1-CAM5), then the sample
223 points are further from the observational site than would be desired. We chose to use sample points
224 in our comparison to observations instead of using regional averages for two main reasons. The
225 first reason is that using regional averages would have lumped together different ice dynamics
226 regimes that should not necessarily be expected to compare well to point observations on landfast
227 ice. The second reason is that we are of the opinion that the resolution in many of these models is

228 sufficiently high to warrant such a direct comparison and provides a better benchmark than
229 regional averages for landfast ice modelling in the CAA.

230 The seasonal cycle (1955-2014) of median ice thickness from CMIP5 (black), ORA-IP
231 models CGLORS, ORAP5.0 and GLORYS2V3 (blue), ECCO-v4 (green) and UR025.4 (red) is
232 shown in Figure 8. ORA-IP models have been split into three groups based, respectively, on their
233 high, medium and low ice thicknesses at Alert. Ice thickness from CMIP5 is comparable to
234 observations (Figure 2) at Cambridge Bay and Resolute with maximum ice thickness reaching 200
235 cm. The ORA-IP models are less consistent. ECCO-v4 tends to have thicker sea ice than
236 observations at Cambridge Bay, Resolute and Eureka but thinner at Alert. CGLORS, ORAP5.0,
237 and GLORYS2V3, on the other hand, are comparable to observations at Cambridge Bay, Resolute
238 and Eureka but have extremely thick and perennial ice close to Alert.

239 The seasonal cycle (1955-2014) of median snow depth from CMIP5 is shown in Figure 9.
240 CMIP5 models indicate a linear increase similar to observations reaching a maximum of ~20 cm
241 in April or May. This is lower than the observed maximum at Resolute, Eureka and Alert but is
242 about twice as much as at Cambridge Bay. While the snow depth reaches zero during the summer
243 at Eureka and Alert in models, the sea ice thickness does not (Figure 8), unlike in observations.
244 This likely reflects the fact that the grid cell thickness in sea ice models with thickness classes a
245 represents the average thickness over these classes. In August the thinner ice classes might have
246 melted but thicker ice classes can still be found, resulting in a substantial average ice thickness
247 over the grid cell. The seasonal cycle over packed ice in these models thus gives a reasonable
248 representation of the seasonal cycle over landfast ice in the CAA, especially in the southern region
249 of the CAA. Overall, this comparison shows how recent improvements in sea ice model resolution

250 allows comparisons with observations that required dynamical downscaling techniques in the
251 previous generation of sea ice models [i.e. *Dumas et al. 2005; Sou and Flato, 2013*].

252 Despite relatively high spatial resolution, PIOMAS does not resolve seasonal ice thickness
253 along the coasts and within the very narrow channels within the CAA (not shown). As a result,
254 Cambridge Bay and Resolute Bay sites represent the only long-term monitoring sites within the
255 CAA suitable for comparison since PIOMAS. The monthly time series of PIOMAS ice and snow
256 thickness estimates at Cambridge Bay and Resolute is shown in Figure 10. The seasonal cycle of
257 ice growth at Cambridge Bay and Resolute is representative compared to observations (Figure 2)
258 but PIOMAS estimates retain more ice in August and September, particularly at Resolute. Ice
259 growth reaches a maximum in April at Cambridge and in May at Resolute which is 1-month earlier
260 compared to observations. Snow depth follows a linear increase similar to observations (Figure 3)
261 with good agreement at Cambridge Bay but considerably underestimates snow depth at Resolute
262 (Figure 10). *Schweiger et al. [2011]* performed a detailed comparison of PIOMAS ice thickness
263 values against *in situ* and Ice, Cloud, and land Elevation Satellite (ICESat) ice thickness
264 observations and found strong correlations. They determined a root mean square error (RMSE) of
265 ~0.76 m and noted that PIOMAS generally overestimates thinner ice and underestimates thicker
266 ice. At both sites within the CAA, PIOMAS ice thickness data is in reasonably good agreement
267 with *in situ* observations with RMSE's of 0.29 cm at Cambridge Bay and 0.68 cm at Resolute
268 (Figure 11). The systematic overestimate of thinner ice reported by *Schweiger et al. [2011]* is more
269 apparent at Resolute than Cambridge Bay (Figure 11). The higher latitude regions of the CAA
270 where there is an intricate mix of seasonal first-year ice and multi-year ice is a problem for
271 PIOMAS and thus contributes to the larger discrepancy at Resolute compared to Cambridge Bay.

272

273 4.2. Trends

274 The spatial distribution of maximum sea ice thickness trends from ORA-IP and CMIP5 is
275 illustrated in Figures 12. The CMIP5 model-mean exhibit a fairly uniform trend pattern, consistent
276 with the different in situ observations (Figure 4) but with overestimated negative thickness trends.
277 Although, for individual models this pattern is far from uniform, the general pattern and magnitude
278 of thickness trends tend to be roughly in accordance with temperature trends (not shown). A similar
279 behavior is observed in the ORA-IP models, with the notable exception of CGLORS, where
280 positive thickness trends are found almost everywhere (Figure 12a). This is robust and it appears
281 that the model is not completely equilibrated in the CAA and exhibit large month-to-month
282 adjustments. Model ORAP5.0 also is not completely equilibrated in the region for years 1979-
283 1984. During those years, it exhibits large inter annual changes in thickness. For this reason, we
284 are only considering years 1985-2013 for this model.

285 For PIOMAS, the North-South overestimated trend is also present (not shown) as with
286 CMIP5 and ORA-IP. Looking specifically at trends computed from 1979-2014 near the observed
287 sites indicates that the mean maximum ice thickness linear trend from at Cambridge Bay is -
288 13.4 ± 3.4 cm decade⁻¹ which is almost double the observational trend of 6.2 ± 2.4 cm decade⁻¹. At
289 Resolute, the PIOMAS linear trend is 24.0 ± 4.1 cm decade⁻¹ which is considerably stronger than
290 the observational trend of -4.9 ± 3.51 cm decade⁻¹.

291

292 4.3. Ice thickness linkages with snow depth and temperature

293 Even though ORA-IP models have unrealistically large thickness trends, the pattern of inter
294 annual correlation (detrended) between winter temperatures and thicknesses is roughly consistent
295 across models (Figure 13). Some ORA-IP models also experience positive correlations (e.g.

296 CGLORS, ORAP5.0, GLORYS2V3 and UR025.4) that are mostly located north of the CAA or
297 within the CAA in regions where multi-year ice is known to be present. It is possible that warmer
298 temperatures are associated with an increased flux of thicker multi-year ice into the CAA which is
299 known to occur [e.g. *Howell et al.*, 2013] but the driving processes responsible for these positive
300 correlations require more investigation. In CMIP5 models, no model exhibits positive correlations
301 with temperature that resemble ORA-IP models over the CAA. Although the time series for the
302 ORA-IP models is short and the positive correlations are only statistically significant at a few grid
303 points in CGLORS and UR025.4, this behavior is sufficiently problematic to recommend that care
304 should be taken when using these ORA-IP models to study the interannual variability in the
305 Canadian Arctic.

306 In the CMIP5 models, significant winter snow depth trends are more strongly negative in
307 the North than in the South (Figure 14). This is in disagreement with point observations presented
308 in the previous sections that showed no significant trends snow depth trends at Alert but negative
309 and significant trends at Cambridge Bay. Although only based on limited point *in situ*
310 observations, this suggests that over the last decades changes in winter precipitation at Alert **must**
311 **have compensated the increased melting driven by increasing temperatures, a compensation that**
312 **is clearly not captured in CMIP5 models.**

313

314 **5. Conclusions**

315 Over the 50+ year *in situ* observational record, statistically significant negative trends in
316 maximum (end-of-winter) ice thickness are present at Cambridge Bay, Eureka and Alert.
317 Significant negative trends in the day of maximum ice thickness are also present at Resolute,
318 Eureka and Alert. Together, these trends suggest thinning of landfast ice in the CAA, where little

319 evidence was found in the shorter record analyzed in an earlier study (BC92). The inter-annual
320 variability of air temperature is only weakly correlated to maximum ice thickness (i.e. maximum
321 correlation is ~0.4). Snow thickness plays the dominant role in controlling maximum ice thickness
322 variability given the high correlations at Resolute and Eureka and reasonably high correlations at
323 Alert and Cambridge Bay.

324 Comparison of CMIP5, ORA-IP and PIOMAS simulations with observations indicate a
325 reasonable representation of the landfast ice thickness monthly climatology within the CAA. This
326 is particularly apparent when seasonal first-year ice dominates the icescape (i.e. Cambridge Bay).
327 Despite improvements in spatial resolution, mixed ice types (i.e. seasonal and multi-year) present
328 at the sub-grid cell resolution are likely problems for model estimates within the CAA. The overall
329 thickness of ice within the CAA in the current generation of models is too high. As a result, trends
330 are unrealistic and far exceed observations (by upwards of $-50 \text{ cm decade}^{-1}$) in part because the
331 initial ice thickness is too large. The problem is particularly acute in the ORA-IP models where
332 large and unrealistic inter annual changes in thickness suggest that the models are not fully
333 equilibrated.

334 ~~Over the mobile Arctic Ocean ice cover, the combined record of submarine and ICESat~~
335 ~~thickness estimates suggest that winter sea ice thickness in the central Arctic has thinned from 3.64~~
336 ~~m in 1980 to 1.75 m by 2009 [Rothrock et al., 2008; Kwok and Rothrock, 2009]—a linear rate of~~
337 ~~over $-60 \text{ cm decade}^{-1}$ that is mostly due to the loss of multi-year ice. However, the contribution of~~
338 ~~seasonal ice to that rate is not available. As seasonal ice, becomes the dominant ice type, the focus~~
339 ~~has shifted to understanding the behavior of seasonal ice thickness. Between 1991 and 2003,~~
340 ~~Melling et al. [2005] found only a small trend ($-7 \text{ cm decade}^{-1}$), though of low statistical~~
341 ~~significance, in the seasonal pack in the Beaufort Sea. In the short ICESat record of ice thickness~~

342 (~~2003–2008~~), *Kwok et al.* [2009] also found negligible trend in the seasonal ice cover. This led
343 them to speculate that a thinner snow cover during to the later start of the growth season is
344 conducive to higher ice production as a result of reduced accumulation of that large fraction of
345 snow that typically falls in October and November. However, over the seasonal ice cover there is
346 the additional contribution of ice deformation on the mean of the thickness distribution.

347 While the impact of the snow cover on ice thickness is well known, the significant
348 correlations at Resolute, Eureka and Alert suggest that the higher sensitivity to changes in snow
349 depth could potentially mask the warming signal on both fast and offshore ice. Thus, even in this
350 limited data set, we can see the dominant role played by snow depth in determining the interannual
351 variability of the maximum landfast ice thickness. This again highlights that the primary factor is
352 the amount and timing of snow accumulation, not air temperature. However, it is worth noting that
353 few of the current generation models show coherent relationships between ice thickness, snow
354 depth and temperature over the longer term record.

355

356 **Authors Contributions**

357 S.E.L.H, F.L and R.K designed the study, performed the analysis and wrote the manuscript with
358 input from C.D. and J.K.

359

360 **Acknowledgements**

361 The authors wish to thank all the individuals responsible for collecting landfast ice and snow
362 thickness measurements in the Canadian Arctic over the past 50+ years.

363

364

365

366

367 **References**

368

369 Alt, B., K. Wilson, and T. Carrieres (2006), A case study of old ice import and export through
370 Peary and Sverdrup channels in the Canadian Arctic Archipelago: 1998-2004, *Ann. Glaciol.*, 44,
371 329–338, doi:10.3189/172756406781811321.

372

373 M.A. Balmaseda , F. Hernandez , A. Storto , M.D. Palmer , O. Alves , L. Shi , G.C. Smith , T.
374 Toyoda , M. Valdivieso , B. Barnier , D. Behringer , T. Boyer , Y-S. Chang , G.A. Chepurin , N.
375 Ferry , G. Forget , Y. Fujii , S. Good , S. Guinehut , K. Haines , Y. Ishikawa , S. Keeley , A.
376 Köhl , T. Lee , M.J. Martin , S. Masina , S. Masuda , B. Meyssignac , K. Mogensen , L. Parent ,
377 K.A. Peterson , Y.M. Tang , Y. Yin , G. Vernieres , X. Wang , J. Waters , R. Wedd , O. Wang ,
378 Y. Xue , M. Chevallier , J-F. Lemieux , F. Dupont , T. Kuragano , M. Kamachi , T. Awaji , A.
379 Caltabiano , K. Wilmer-Becker , F. Gaillard, The Ocean Reanalyses Intercomparison Project
380 (ORA-IP), *Journal of Operational Oceanography*, Vol. 8, Iss. sup1, 2015,
381 DOI:10.1080/1755876X.2015.1022329

382

383 Brown, R., and P. Cote (1992), Interannual variability of landfast ice thickness in the Canadian
384 high arctic, 1950–89. *Arctic*, 45, 273–284.

385

386 Bromwich, D. H., A. B. Wilson, L. Bai, G. W. K. Moore, and P. Bauer, 2015: A comparison of
387 the regional Arctic System Reanalysis and the global ERA-Interim Reanalysis for the Arctic. *Q.*
388 *J. R. Meteorol. Soc.*, doi: 10.1002/qj.2527

389

390 Dee DP, co-authors (2011), The ERA-Interim reanalysis: configuration and performance of the
391 data assimilation system. *Q J R Meteorol Soc.* 137: 553–597, doi:10.1002/qj.828.

392

393 Dumas, J. A., G. M. Flato, and R. D. Brown (2006), Future projections of landfast ice thickness
394 and duration in the Canadian Arctic. *J. Climate*, 19, 5175–5189.

395

396 Druckenmiller, M. L., H. Eicken, M. A. Johnson, D. J. Pringle, and C. C. Williams (2009),
397 Toward an integrated coastal sea-ice observatory: System components and a case study at
398 Barrow, Alaska. *Cold Reg.Sci.Tech.*, 56, 61-72.

399

400 Flato, G. M., and R. D. Brown (1996), Variability and climate sensitivity of landfast Arctic sea
401 ice. *J. Geophys. Res.*, 101 (C10), 25 767–25 777.

402

403 Forget, G., Campin, J.-M., Heimbach, P., Hill, C. N., Ponte, R. M., and Wunsch, C. (2015),
404 ECCO version 4: an integrated framework for non-linear inverse modeling and global ocean
405 state estimation, *Geosci. Model Dev.*, 8, 3071-3104, doi:10.5194/gmd-8-3071-2015/

406

407 Gerland, S., A. H. H. Renner, F. Godtlielsen, D. Divine, and T. B. Loynning (2008), Decrease of
408 sea ice thickness at Hopen, Barents Sea, during 1966-2007. *Geophys. Res. Lett.*, 35, L06501.

409

410 Gough, W., A.S. Gagnon an H.P Lau (2004), Interannual variability of Hudson Bay Ice
411 Thickness, *Polar Geography*, 28(3), 222-238.

412

413 Haines K, M. Valdivieso, H. Zuo, and V.N. Stepanov (2012), Transports and budgets in a 1/4 °
414 global ocean reanalysis 1989–2010. *Ocean Sci.* 8(3): 333–344, doi:10.5194/os-8-333-
415 2012.002/qj.2063.

416
417 Haas, C., and S. E. L. Howell (2015), Ice thickness in the Northwest Passage, *Geophys. Res.*
418 *Lett.*, 42, doi:10.1002/2015GL065704

419
420 Howell, S. E. L., C. R. Duguay, and T. Markus (2009), Sea ice conditions and melt season
421 duration variability within the Canadian Arctic Archipelago: 1979–2008, *Geophys. Res. Lett.*,
422 36, L10502, doi:10.1029/2009GL037681.

423 Howell, S. E. L., T. Wohleben, M. Daboor, C. Derksen, A. Komarov, and L. Pizzolato (2013),
424 Recent changes in the exchange of sea ice between the Arctic Ocean and the Canadian Arctic
425 Archipelago, *J. Geophys. Res. Oceans*, 118, 3595–3607, doi:10.1002/jgrc.20265.

426 Jeffers, S., T. Agnew, B. Alt, R. De Abreu, and S. McCourt (2001), Investigating the anomalous
427 sea ice conditions in the Canadian High Arctic (Queen Elizabeth Islands) during the summer of
428 1998, *Ann. Glaciol.*, 33, 507– 612.

429
430 Jeffries, M. O. and J. Richter-Menge, Eds. (2015), The Arctic [in State of the Climate in 2014],
431 *Bull. Amer. Meteor. Soc.*, 96, ES1–ES32.
432 doi: <http://dx.doi.org/10.1175/2015BAMSStateoftheClimate.1>

433
434 Jones, P.D., T.M.L. Wigley, C.K. Folland and D.E. Parker (1987), Spatial patterns in recent
435 worldwide temperature trends. *Climate Monitor*, 16(5): 175-185.

436
437 Jones, P.D., M. New, D.E. Parker, S. Martin, and I.G. Rigor (1999), Surface air temperature and
438 its changes over the past 150 years, *Rev. Geophys.*, 37(2),173–200.

439
440 Kwok, R., and D. A. Rothrock (2009), Decline in Arctic sea ice thickness from submarine and
441 ICESat records: 1958 – 2008, *Geophys. Res. Lett.*, 36, L15501, doi:10.1029/2009GL039035.

442
443 Laliberté, F., S. E. L. Howell, and P. J. Kushner (2016), Regional variability of a projected sea
444 ice-free Arctic during the summer months, *Geophys. Res. Lett.*, 43, 256–263,
445 doi:10.1002/2015GL066855.

446
447 Laxon S. W., K. A. Giles, A. L. Ridout, D. J. Wingham, R. Willatt, R. Cullen, R. Kwok, A.
448 Schweiger, J. Zhang, C. Haas, S. Hendricks, R. Krishfield, N. Kurtz, S. Farrell and M. Davidson
449 (2013), CryoSat-2 estimates of Arctic sea ice thickness and volume, *Geophys. Res. Lett.*, 40,
450 732–737, doi:10.1002/grl.50193.

451
452 Masina, S. et al. (2015), An ensemble of eddy-permitting global ocean reanalyses from the
453 MyOcean project. *Clim. Dynam.* 1–29, doi:10.1007/s00382-015-2728-5

454
455 Mahoney, A., H. Eicken, and L. Shapiro (2007), How fast is landfast sea ice? A study of the
456 attachment and detachment of nearshore ice at Barrow, Alaska. *Cold Reg.Sci.Tech.*, 47, 233-255.

457

458 Mahoney, A. R., H. Eicken, A. G. Gaylord, and R. Gens (2014), Landfast sea ice extent in the
459 Chukchi and Beaufort seas: The annual cycle and decadal variability, *Cold Reg. Sci. Technol.*,
460 103, 41–56, doi:10.1016/j.coldregions.2014.03.003.

461 Melling, H. (2002), Sea ice of the northern Canadian Arctic Archipelago, *J. Geophys. Res.*,
462 107(C11), 3181, doi:10.1029/2001JC001102.

463
464 Melling, H., C. Haas, and E. Brossier (2015), Invisible polynyas: Modulation of fast ice
465 thickness by ocean heat flux on the Canadian polar shelf, *J. Geophys. Res. Oceans*, 120, 777–
466 795, doi:10.1002/2014JC010404.

467 Ólason, E. Ö. (2012), Dynamical modeling of Kara Sea land-fast ice, PhD thesis, Univ. of
468 Hamburg, Hamburg, Germany.

469
470 Polyakov, I. V., et al. (2010), Arctic Ocean Warming Contributes to Reduced Polar Ice Cap.
471 *Journal of Physical Oceanography*, 40, 2743-2756

472
473 Schweiger, A., R. Lindsay, J. Zhang, M. Steele, H. Stern, and R. Kwok (2011), Uncertainty in
474 modeled Arctic sea ice volume, *J. Geophys. Res.*, 116, C00D06, doi:10.1029/2011JC007084.

475
476 Serson, H.V. (1972), Investigations of a plug of multiyear old sea ice in the mouth of Nansen
477 Sound. Ottawa, Ont., Department of National Defence, Canada. Defence Research Establishment
478 Ottawa. (DREO Tech. Note 72-6.)

479
480 Serson, H.V. (1974), Sverdrup Channel. Ottawa, Ont., Department of National Defence, Canada.
481 Defence Research Establishment Ottawa. (DREO Tech. Note 74-10.)

482
483 Sou, T., and G. Flato (2009), Sea ice in the Canadian Arctic Archipelago: Modeling the past
484 (1950-2004) and the future (2041-60), *J. Clim.*, 22, 2181–2198, doi:10.1175/2008JCLI2335.1

485 Stroeve, J. C., M. C. Serreze, M. M. Holland, J. E. Kay, J. Malanik, and A. P. Barrett (2011),
486 The Arctic’s rapidly shrinking sea ice cover: A research synthesis, *Clim. Change*, 110(3-4),
487 1005–1027.

488
489 Storto A, S. Dobricic S, S. Masina and D. Di Pietro (2011), Assimilating along-track altimetric
490 observations through local hydrostatic adjustments in a global ocean reanalysis system. *Mon*
491 *Wea Rev.* 139: 738–754.

492
493 Stroeve, J. C., M. C. Serreze, M. M. Holland, J. E. Kay, J. Maslanik, and A. P. Barrett (2012),
494 The Arctic’s rapidly shrinking sea ice cover: A research synthesis, *Clim. Change*, 110(3–4),
495 1005–1027

496
497 Swart, N. C., J. C. Fyfe, E. Hawkins, J. E. Kay, and A. Jahn (2015), Influence of internal
498 variability on Arctic sea-ice trends, *Nat. Clim. Change*, 5, 86–89, doi:10.1038/nclimate2483.

499
500 Taylor, K. E., R. J. Stouffer, and G. A. Meehl (2012), An overview of CMIP5 and the
experiment design, *Bull. Am. Meteorol. Soc.*, 93, 485–498, doi:10.1175/BAMS-D-11-00094.1.

501
502 Tivy, A., S. E. L. Howell, B. Alt, S. McCourt, R. Chagnon, G. Crocker, T. Carrieres, and J. J.
503 Yackel (2011), Trends and variability in summer sea ice cover in the Canadian Arctic based on
504 the Canadian Ice Service Digital Archive, 1960–2008 and 1968–2008, *J. Geophys. Res.*, 116,
505 C03007, doi:10.1029/2009JC005855.
506
507 Vincent, L., X. Wang, E. Milewska, Hui Wan, F. Yang, and V. Swail (2012), A second
508 generation of homogenized Canadian monthly surface air temperature for climate trend analysis.
509 *Journal of Geophysical Research*, D18110, doi:10.1029/2012JD017859
510
511 Warren, S. G., I. G. Rigor, N. Untersteiner, V. F. Radionov, N. N. Bryazgin, Y. I. Aleksandrov,
512 and R. Colony (1999), Snow depth on Arctic sea ice, *J. Clim.*, 12, 1814– 1829.
513
514 Wilks, D. S. (2006). On “field significance” and the false discovery rate. *J. Appl. Meteor.*
515 *Climatol.*, 45, 1181–1189. doi: <http://dx.doi.org/10.1175/JAM2404.1>
516 Woo, M-K., and R. Heron (1989), Freeze-up and break-up of ice cover on small arctic lakes. In:
517 Mackay, W.C., ed. Northern lakes and rivers. Edmonton: Boreal Institute for Northern Studies,
518 56-62.
519
520 Woo, M-K., R. Heron, P. Marsh, and P. Steer, (1983), Comparison of weather station snowfall
521 with winter snow accumulation in High Arctic basins, *Atmos.-Ocean*, 21(3):312-325.
522
523 World Meteorological Organization, (1970), WMO sea-ice nomenclature. Terminology, codes
524 and illustrated glossary. WMO/OMM.BMO No. 259, 145 pp, Geneva Secretariat of the World
525 Meteorological Organization
526
527 Yu, Y, H. Stern, C. Fowler, F. Fetterer, and J. Maslanik (2014), Interannual Variability of Arctic
528 Landfast Ice between 1976 and 2007. *J. Climate*, **27**, 227–243.
529 doi: <http://dx.doi.org/10.1175/JCLI-D-13-00178.1>
530
531 Zhang, J.L. and D.A. Rothrock, (2003), Modeling global sea ice with a thickness and enthalpy
532 distribution model in generalized curvilinear coordinates, *Mon. Weather Rev.*, 131, 845-861.
533 Zuo, H., M.A. Balmaseda, and K. Mogensen (2015), The new eddy-permitting ORAP5 ocean
534 reanalysis: description, evaluation and uncertainties in climate signals. *Clim. Dynam.* 1–21.
535 doi:10.1007/s00382-015-2675-1.
536
537
538
539
540
541
542
543
544
545
546

547 Table 1. CMIP5 models used in this study, the number of realizations with ice data and the
 548 number of realizations with sea ice transport data

	w/ ice		w/ ice
bcc-csm1-1	1	MIROC-ESM-CHEM	1
bcc-csm1-1-m	1	MIROC5	3
BNU-ESM	1	HadGEM2-CC	1
CanESM2	5	HadGEM2-ES	4
CMCC-CESM	1	MPI-ESM-LR	3
CMCC-CM	1	MPI-ESM-MR	1
CMCC-CMS	1	MRI-CGCM3	1
CNRM-CM5	5	CCSM4	6
ACCESS1.0	1	NorESM1-M	1
ACCESS1.3	1	NorESM1-ME	1
CSIRO-Mk3.6.0	10	GFDL-CM3	1
FIO-ESM	1	GFDL-ESM2G	1
EC-EARTH	6	GFDL-ESM2M	1
inmcm4	1	CESM1(BGC)	1
FGOALS-g2	1	CESM1(CAM5)	3
MIROC-ESM	1	CESM1(WACCM)	3

549
 550
 551
 552
 553
 554
 555
 556
 557
 558
 559
 560
 561
 562
 563
 564
 565
 566
 567

568 Table 2. Summary of ORA-IP models characteristics

Model Name	CGLORS	ECCO-v4	GLORYS2V3	ORAP5.0	UR025.4	PIOMASS
Institute	CMCC	JPL-NASA-MIT-AER	Mercator Océan	ECMWF	University of Reading	APL/PSC
Resolution	ORCA0.25°	~40km in the Arctic	ORCA0.25°	ORCA0.25°	ORCA0.25°	~22km in the Arctic
Ocean Model	NEMO 3.2.1	MITgcm	NEMO 3.1	NEMO3.4	NEMO 3.2	POP
Sea ice Model	LIM2	MITgcm	LIM2 (with EVP rheology)	LIM2	LIM2	TED
Time period considered	1982-2012	1991-2011	1993-2013	1985-2013	1993-2010	1958-2015
Atmospheric forcing	ERA-Interim	ERA-Interim	ERA-Interim	ERA-Interim	ERA-Interim	NCEP/NCAR
Sea ice product assimilated	NSIDC NASA-Team Daily	NSIDC Bootstrap Monthly	IFREMER/CERSAT	NOAA / OSTIA combination	EUMETSAT OSI-SAF	NSIDC near-real time Daily

569
570
571
572
573
574
575
576
577
578
579
580
581
582
583
584
585
586
587
588
589
590
591
592
593

594 Table 3. Observed maximum ice thickness, snow depth, and surface air temperature at four
 595 landfast ice sites in the Canadian Arctic Archipelago. The bold text indicates statistical
 596 significance of the linear trend at 95% or greater.

	Cambridge Bay	Resolute	Eureka	Alert
Period	1960-2014	1957-2014	1957-2014	1957-2014
Ice Thickness, h_{ice}				
Mean of $max h_{ice}$ (m)	2.11±0.19	2.02±0.19	2.27±0.23	1.98±0.22
Trend of $max h_{ice}$ (cm decade ⁻¹)	-4.31±1.4	-0.5±1.6	-4.65±1.7	-4.44±1.6
Day of $max h_{ice}$	24 May±17	25 May±21	26 May±12	27 May±16
Trend of day of $max h_{ice}$ (days decade ⁻¹)	-0.87±1.5	-6.2±1.5	-2.0±0.1	-3.0±1.2
Snow depth (h_{snow})				
Mean Oct-May h_{snow} (cm)	8.4±4.2	22.6±10	17.6±5.8	18.4±6.2
Trend of Oct-May h_{snow} (cm decade ⁻¹)	-0.8±0.4	-0.75±0.8	0.54±0.5	0.26±0.5
Temperature				
Winter (Dec-Feb) Mean (°C)	-31.3±2.0	-30.8±1.9	-36.0±2.0	-31.2±1.6
Winter (Dec-Feb) (°C/decade)	0.59±0.2	0.35±0.1	0.23±0.2	0.38±0.1
Spring (Mar-May) Mean (°C)	-20.0±1.8	-21.1±1.8	-24.9±2.0	-22.8±1.8
Spring (Mar-May) (°C/decade)	0.47±0.1	0.57±0.1	0.44±0.1	0.32±0.1
Summer (Jun-Aug) Mean (°C)	5.9±1.4	2.3±1.3	3.9±1.2	1.3±0.8
Summer (Jun-Aug) (°C/decade)	0.30±0.1	0.17±0.2	0.21±0.1	0.1±0.1
Fall (Sep-Nov) Mean (°C)	-11.1±2.0	-13.8±2.0	-19.6±2.2	-18.0±1.7
Fall (Sep-Nov) (°C/decade)	0.60±0.2	0.67±0.1	0.68±0.2	0.56±0.1

597
 598
 599
 600
 601
 602

603 **List of Figures**

604

605 Figure 1. Map of the central Canadian Arctic Archipelago showing the location of the landfast
606 snow and thickness observations.

607

608 Figure 2. Seasonal cycle of observed mean ice thickness at the four sites (1960-2014).

609

610 Figure 3. Seasonal cycle of observed mean snow depth at the four sites (1960-2014).

611

612 Figure 4. Time series and trend of observed maximum ice thickness at the four sites.

613

614 Figure 5. Time series and trend of observed mean October through May snow depth at the four
615 sites.

616

617 Figure 6. Weekly time series of ice thickness and snow depth at Eureka and Alert for (a) low
618 snow years and (b) high snow years.

619

620 Figure 7. Time series of mean air temperature during winter (DJF), spring, (MAM), summer
621 (JJA) and autumn (SON) at the four sites.

622

623 Figure 8. CMIP5 median sea ice thickness seasonal cycle (1955-2014) at stations (grey).
624 Observations from 2 (black). Median of ORA-IP models CGLORS, ORAP5.0, GLORYS2V3
625 (blue), ECCO-v4 (green) and UR025.4 (red). Whiskers indicate the 5th and 95th percentiles.

626

627 Figure 9. Same as Figure 8 for snow depth and only for CMIP5 models (grey) and observations
628 (black).

629

630 Figure 10. Seasonal cycle of observed mean ice thickness (left) and snow depth (right) from
631 PIOMAS at Cambridge Bay and Resolute (1979-2014).

632

633 Figure 11. Comparison of PIOMAS ice thickness with ice thickness observations from
634 Environment Canada's ice thickness monitoring sites at Cambridge Bay and Resolute. The data
635 covers the period 1979-2014.

636

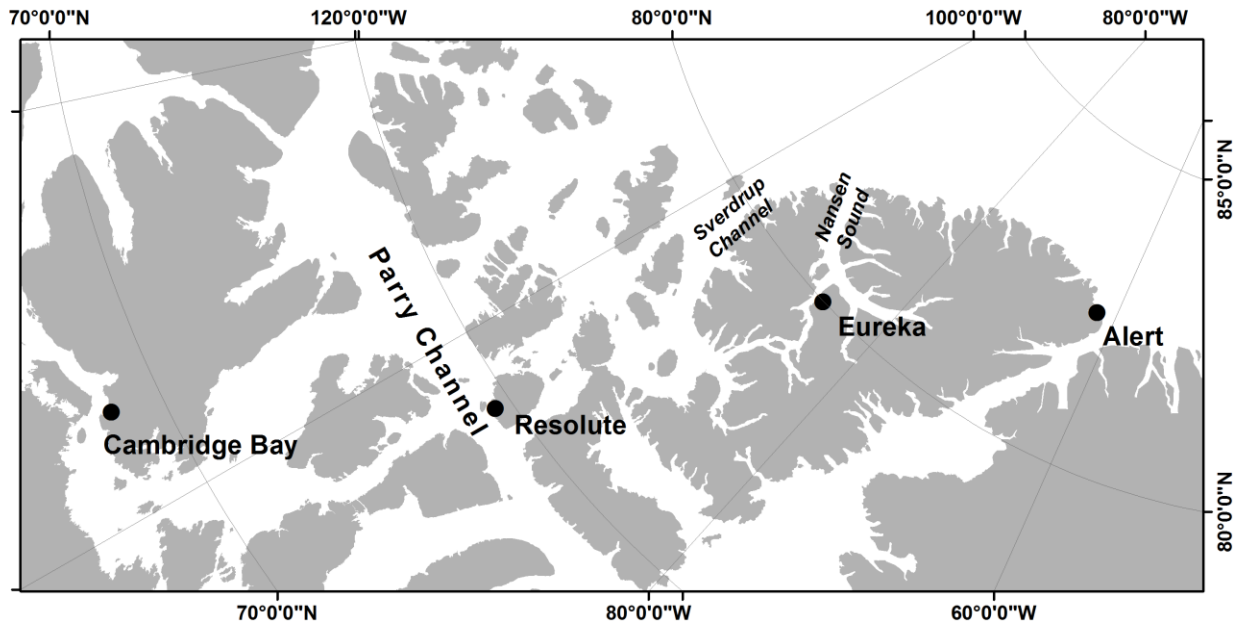
637 Figure 12. **a-e:** Maximum sea ice thickness trends in ORA-IP simulations. **f:** Same for CMIP5
638 MODEL-MEAN. From South to North, o's indicate Cambridge Bay (green), Resolute (blue),
639 Eureka (white) and Alert (black) and x's indicate the corresponding measurement stations. In **f**,
640 one o per model is shown." The stippling indicates p-values less than 0.05, corrected using the
641 False Discovery Rate (FDR) method with a global pFDR-values less than 0.10 [Wilks, 2006].
642 The colorbar is linear from -10 cm dec-1 to 10 cm dec-1 and symmetric logarithmic beyond
643 these values.

644

645 Figure 13. **a-e:** Pearson correlation of detrended maximum sea ice thickness in ORA-IP with
646 detrended ONDJFMAM ERA-INTERIM 2m temperature. **f:** Same but for CMIP5 MODEL-
647 MEAN. The stippling indicates p-values less than 0.05, corrected using the False Discovery Rate
648 (FDR) method with a global pFDR-values less than 0.10 [Wilks, 2006].

649
650
651
652
653
654
655
656
657
658
659
660
661
662
663
664
665
666
667
668
669
670
671
672
673
674
675
676
677
678
679
680
681
682
683
684
685
686
687
688
689

Figure 14. Same as Figure 12f but for snow depth trends (ONDFJMAM).



690
 691
 692
 693
 694
 695
 696
 697

Figure 1. Map of the central Canadian Arctic Archipelago showing the location of the landfast snow and thickness observations.

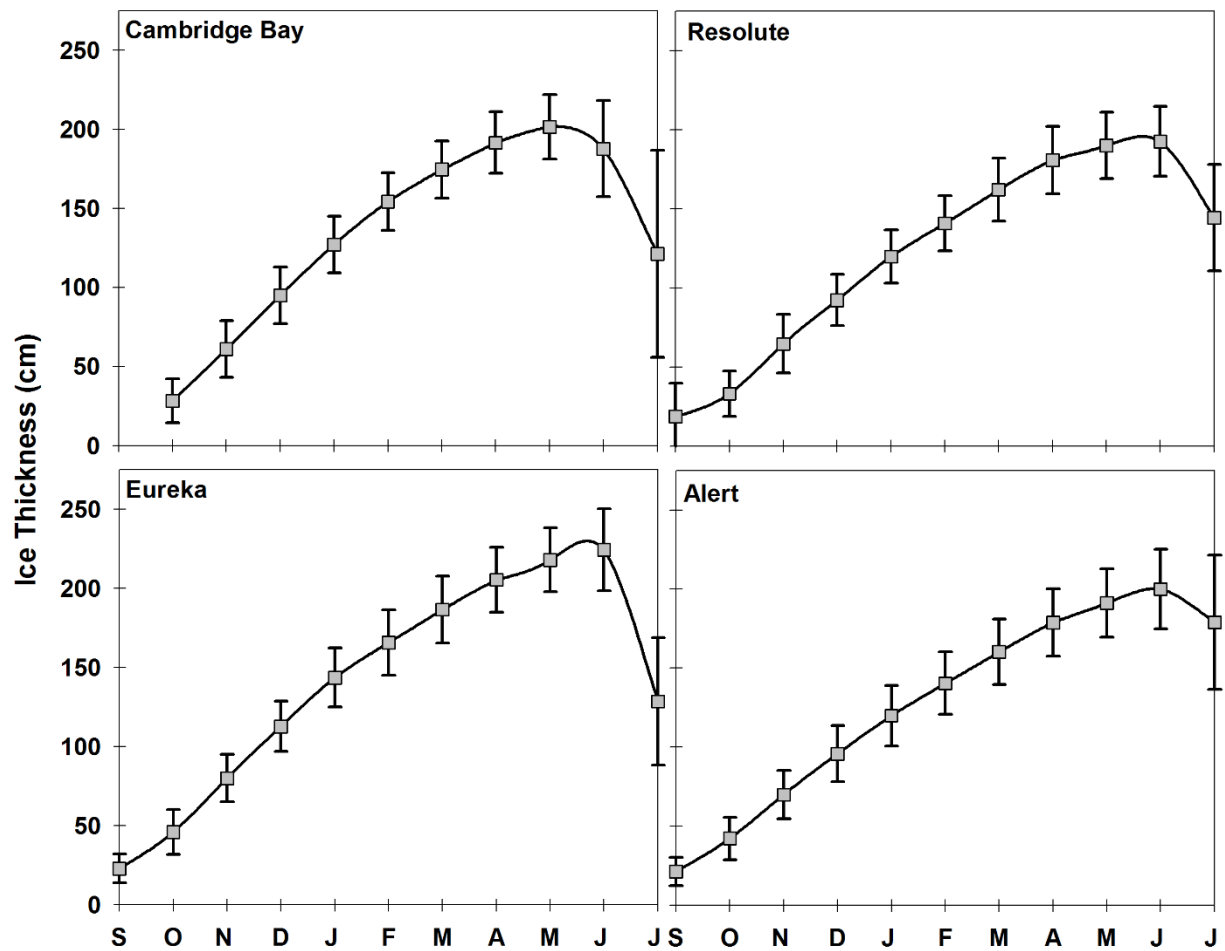


Figure 2. Seasonal cycle of observed mean ice thickness at the four sites (1960-2014).

698
 699
 700
 701
 702
 703
 704
 705
 706
 707
 708

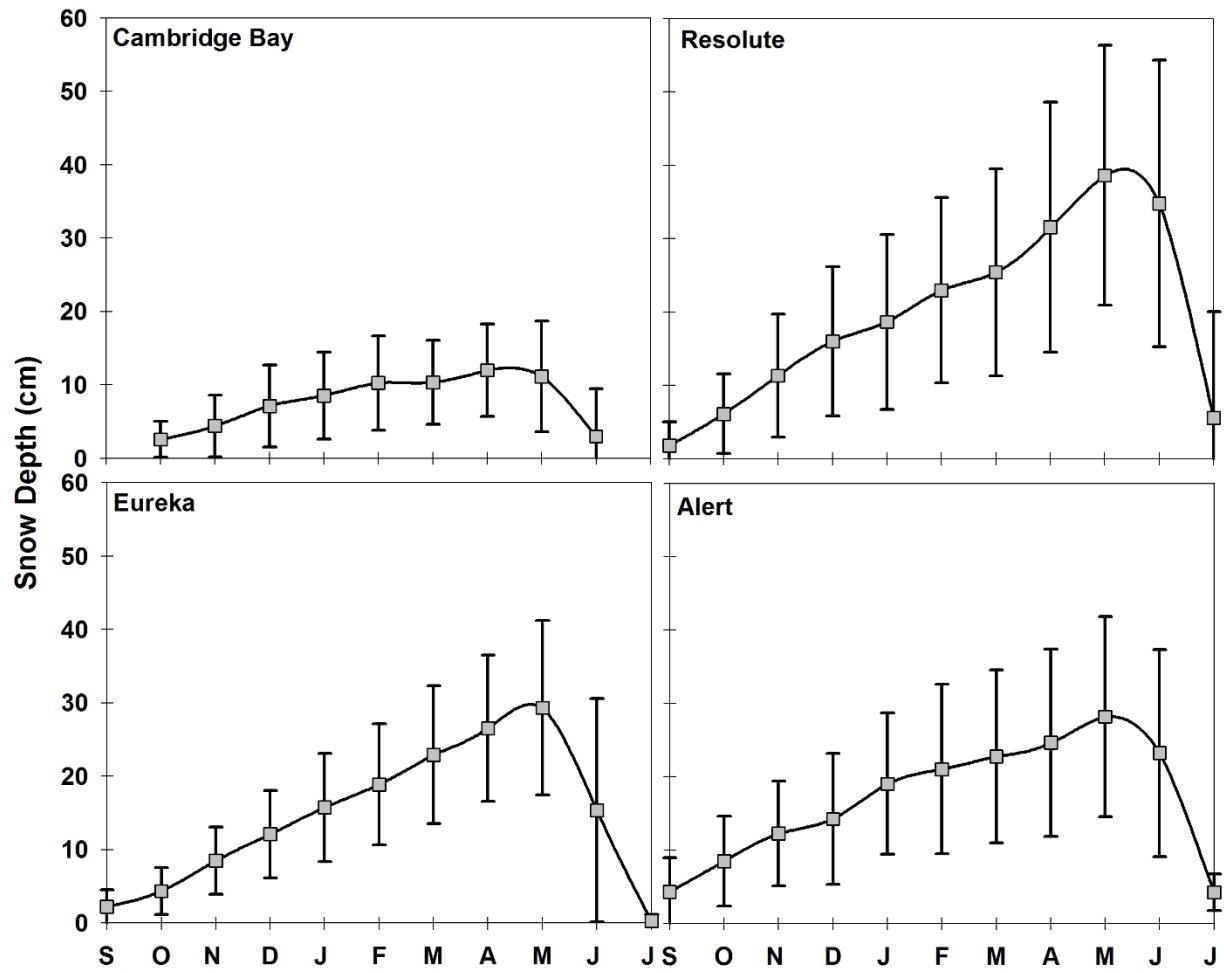


Figure 3. Seasonal cycle of observed mean snow depth at the four sites (1960-2014).

709
 710
 711
 712
 713
 714
 715

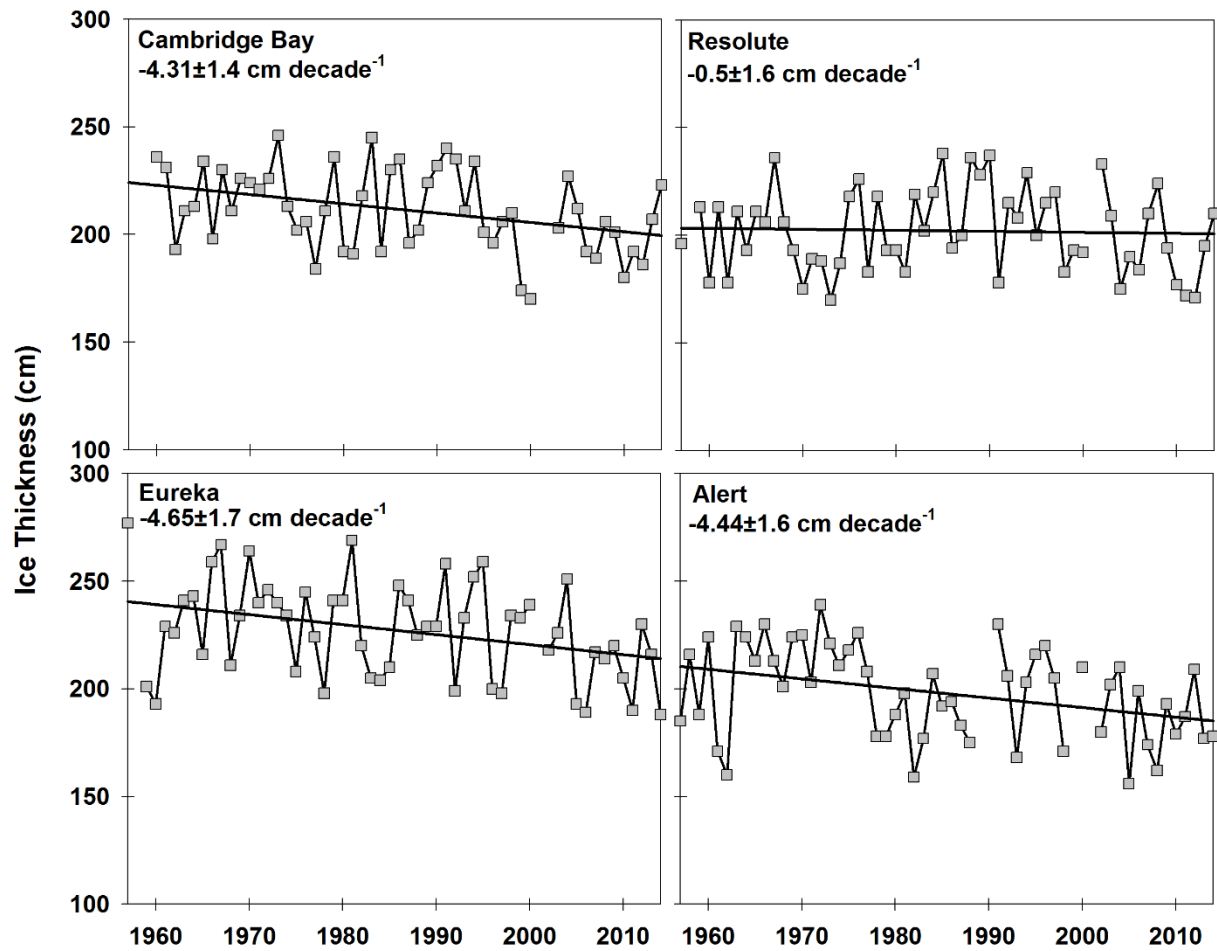
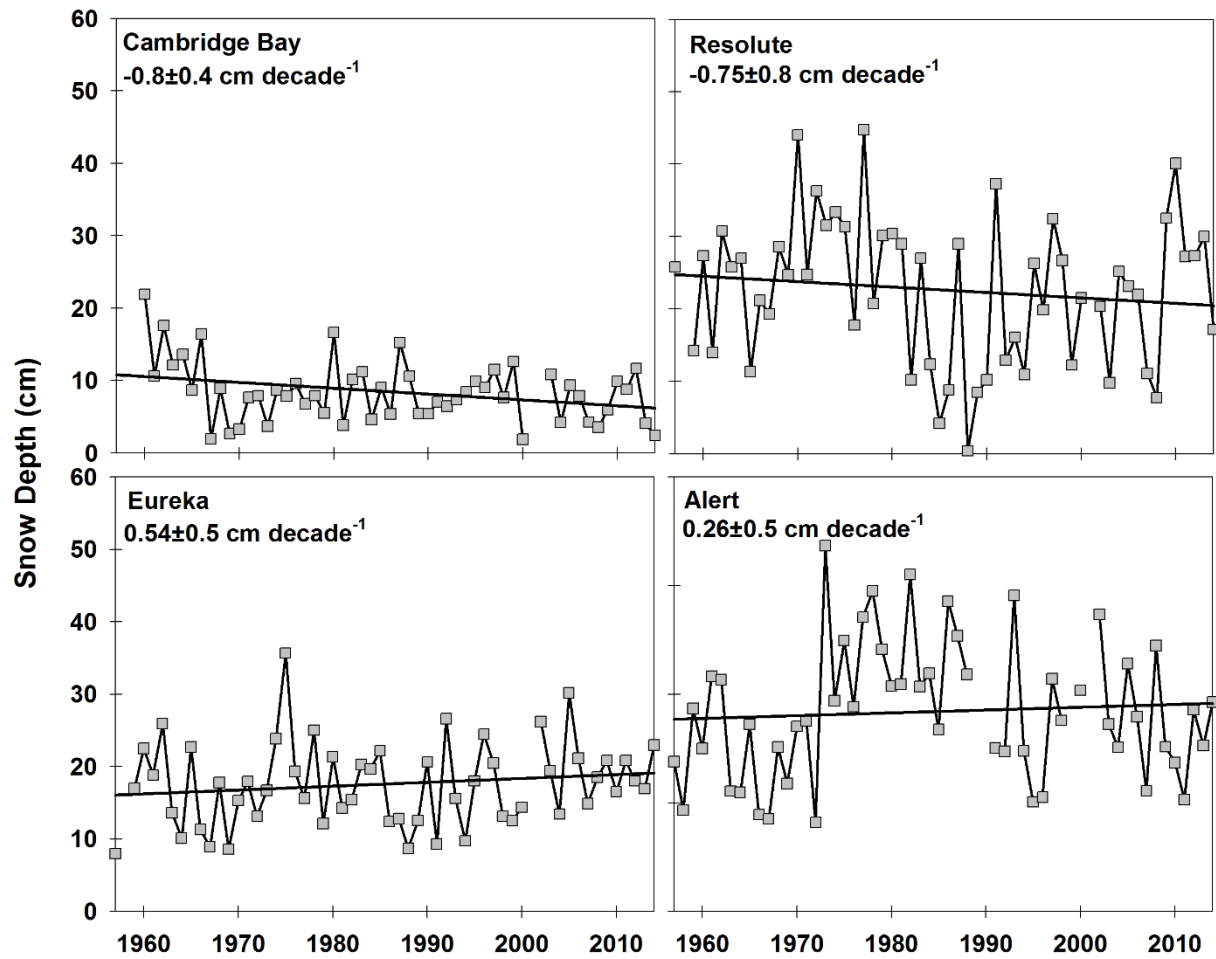


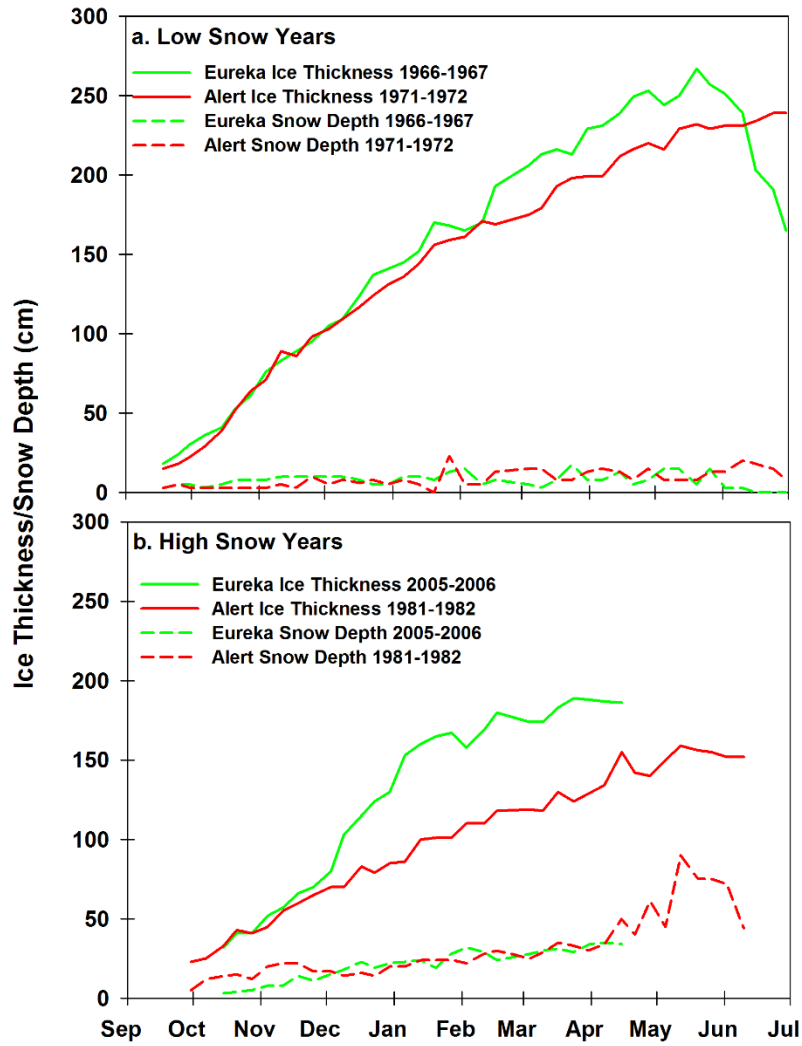
Figure 4. Time series and trend of observed maximum ice thickness at the four sites.

716
 717
 718
 719
 720
 721
 722
 723
 724
 725



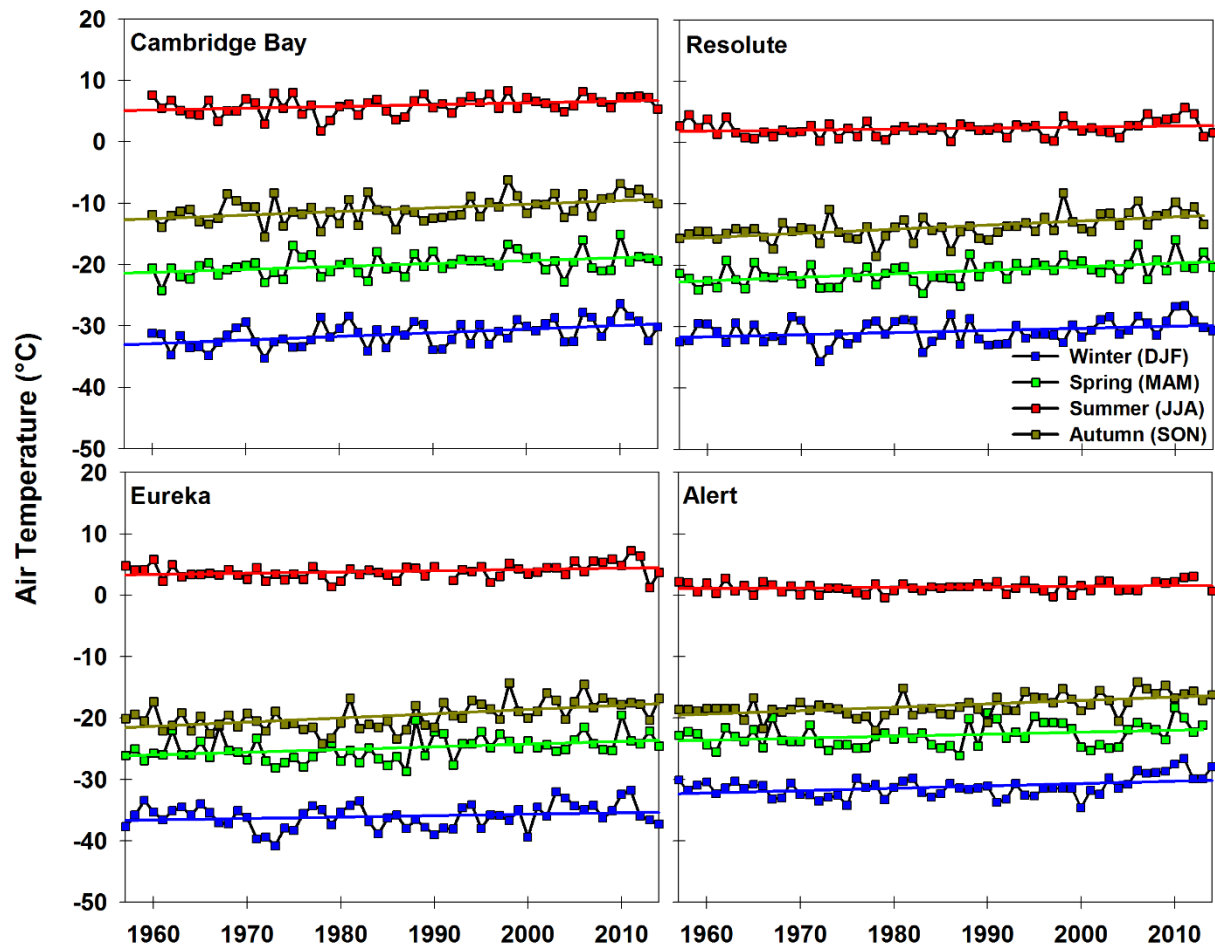
726
 727
 728
 729
 730
 731
 732
 733
 734

Figure 5. Time series and trend of observed mean October through May snow depth at the four sites.



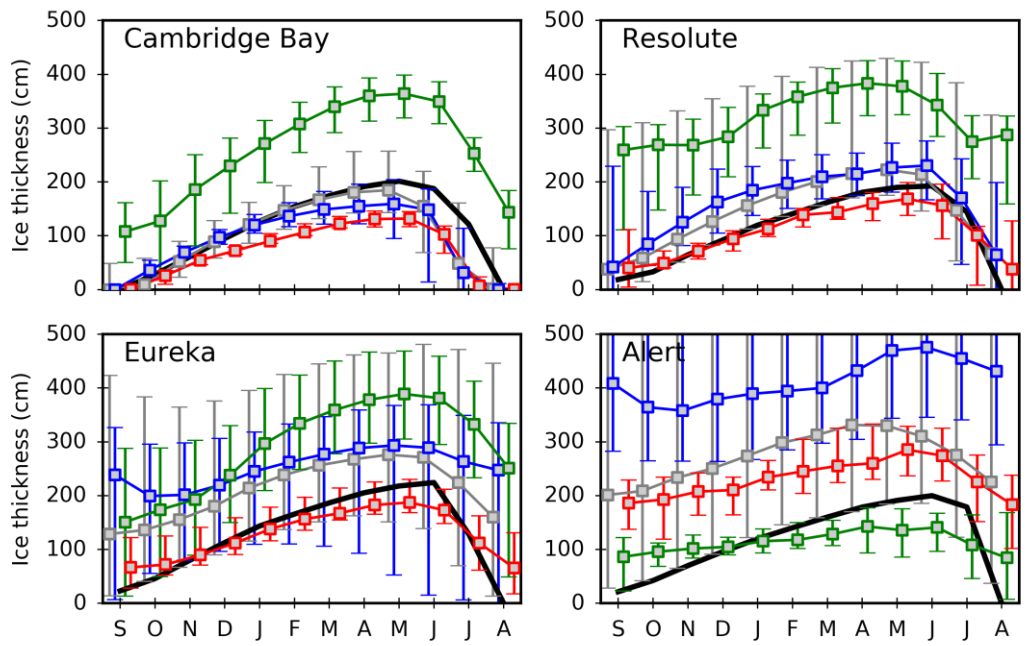
735
 736 Figure 6. Weekly time series of ice thickness and snow depth at Eureka and Alert for (a) low
 737 snow years and (b) high snow years.

738
 739
 740
 741

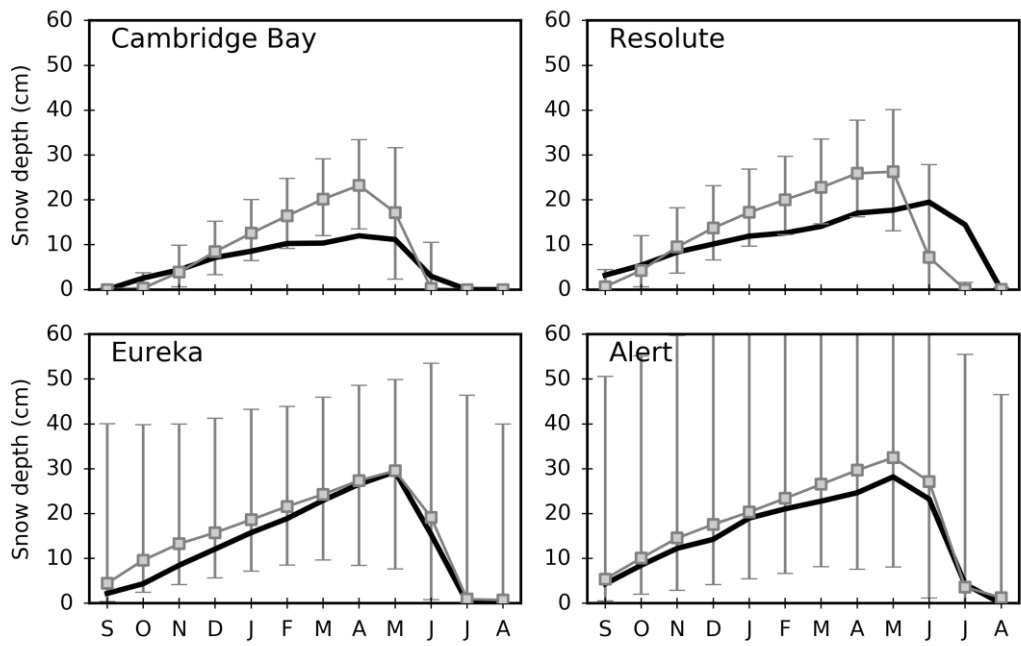


742
 743 Figure 7. Time series of mean air temperature during winter (DJF), spring, (MAM), summer
 744 (JJA) and autumn (SON) at the four sites.

745
 746
 747
 748
 749

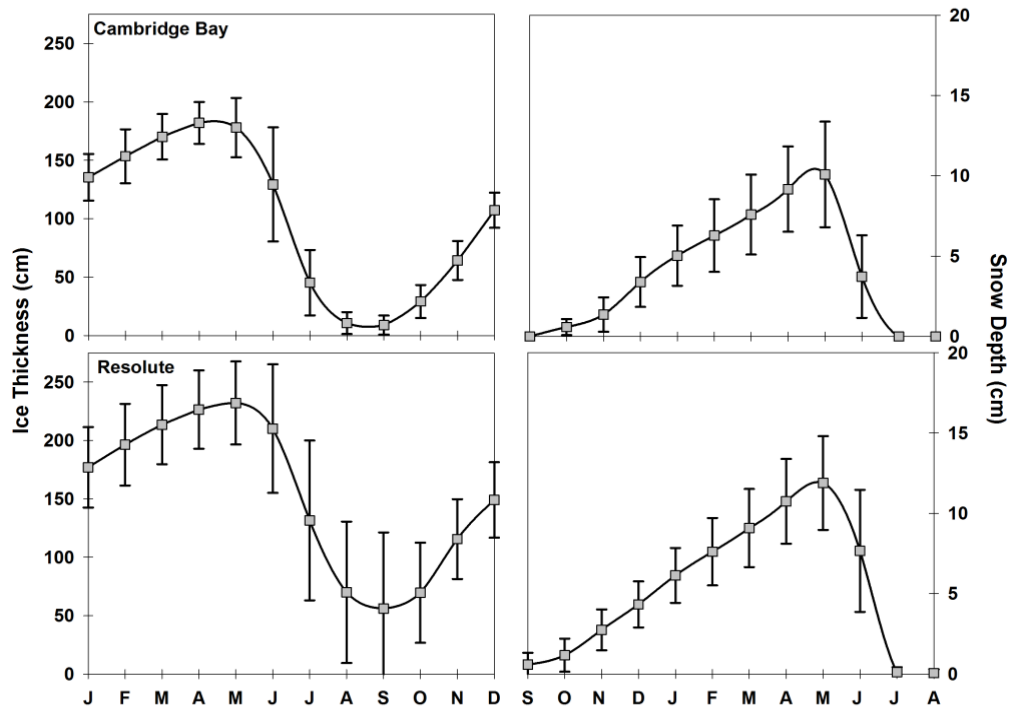


750
 751 Figure 8. CMIP5 median sea ice thickness seasonal cycle (1955-2014) at stations (grey).
 752 **Observations from 2 (black)**. Median of ORA-IP models CGLORS, ORAP5.0, GLORYS2V3
 753 (blue), ECCO-v4 (green) and UR025.4 (red). Whiskers indicate the 5th and 95th percentiles.
 754
 755
 756
 757
 758



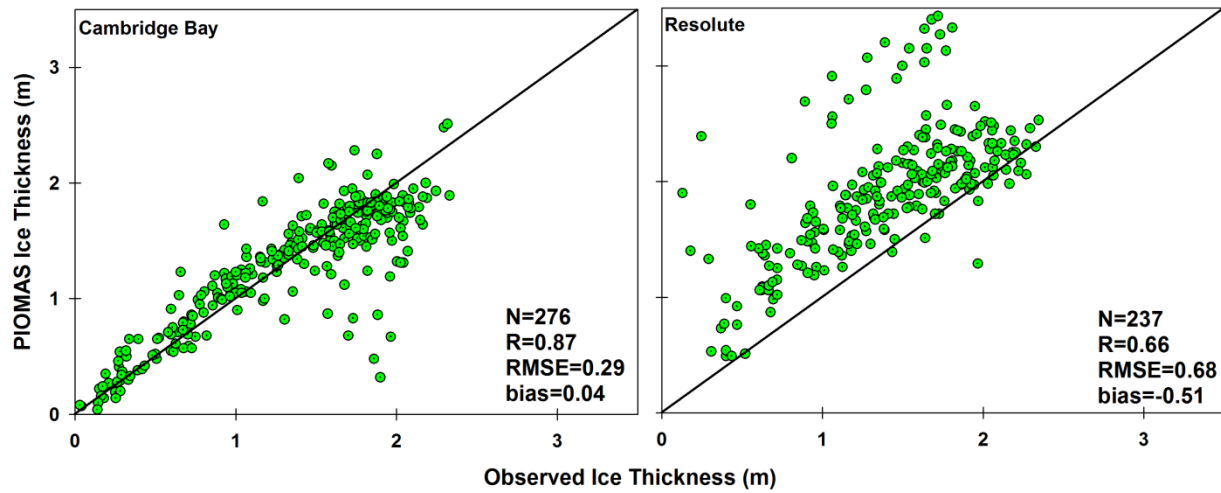
759
 760
 761
 762
 763
 764
 765
 766
 767
 768
 769
 770
 771
 772
 773
 774
 775
 776
 777
 778
 779
 780
 781
 782
 783
 784
 785

Figure 9. Same as Figure 8 for snow depth and only for CMIP5 models (grey) and observations (black).

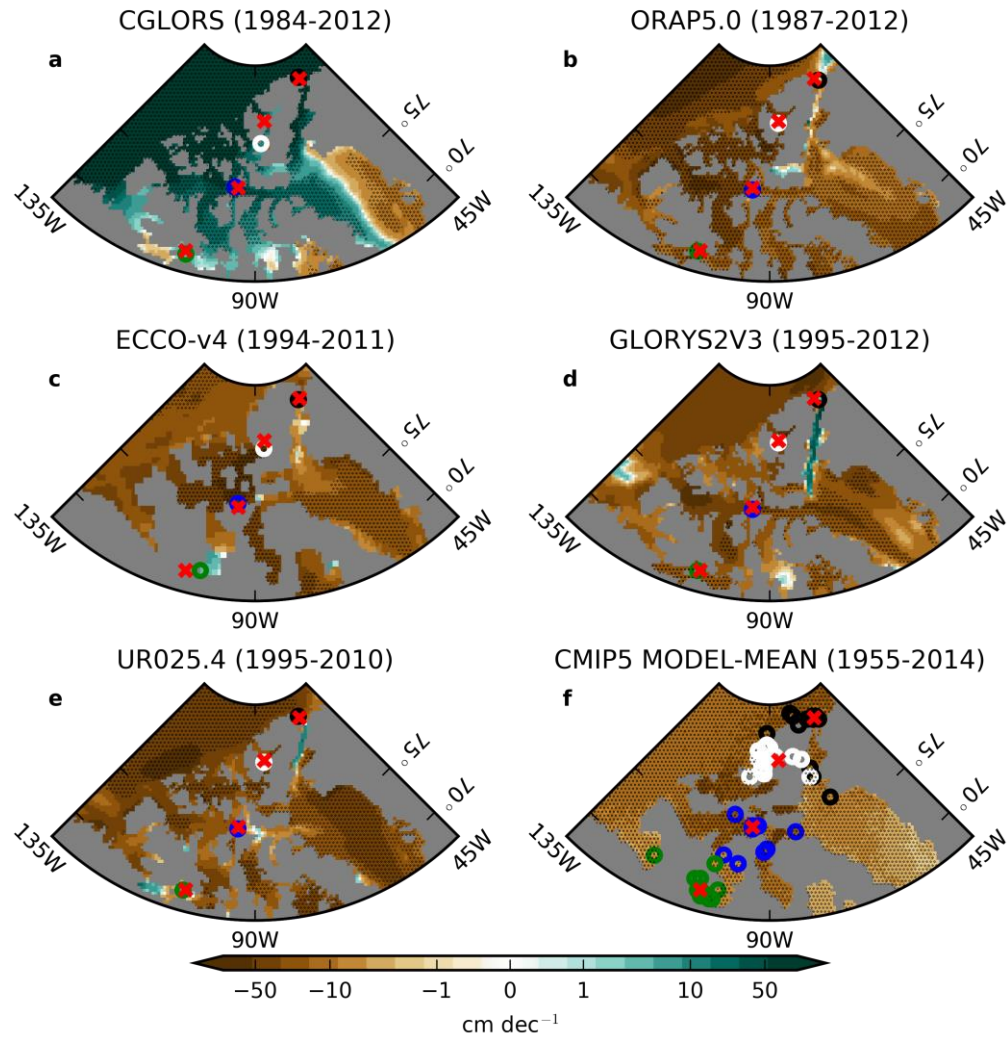


786
 787 Figure 10. Seasonal cycle of observed mean ice thickness (left) and snow depth (right) from
 788 PIOMAS at Cambridge Bay and Resolute (1979-2014).
 789

790
 791
 792
 793
 794
 795
 796
 797
 798
 799
 800
 801
 802
 803
 804
 805
 806
 807
 808
 809
 810
 811

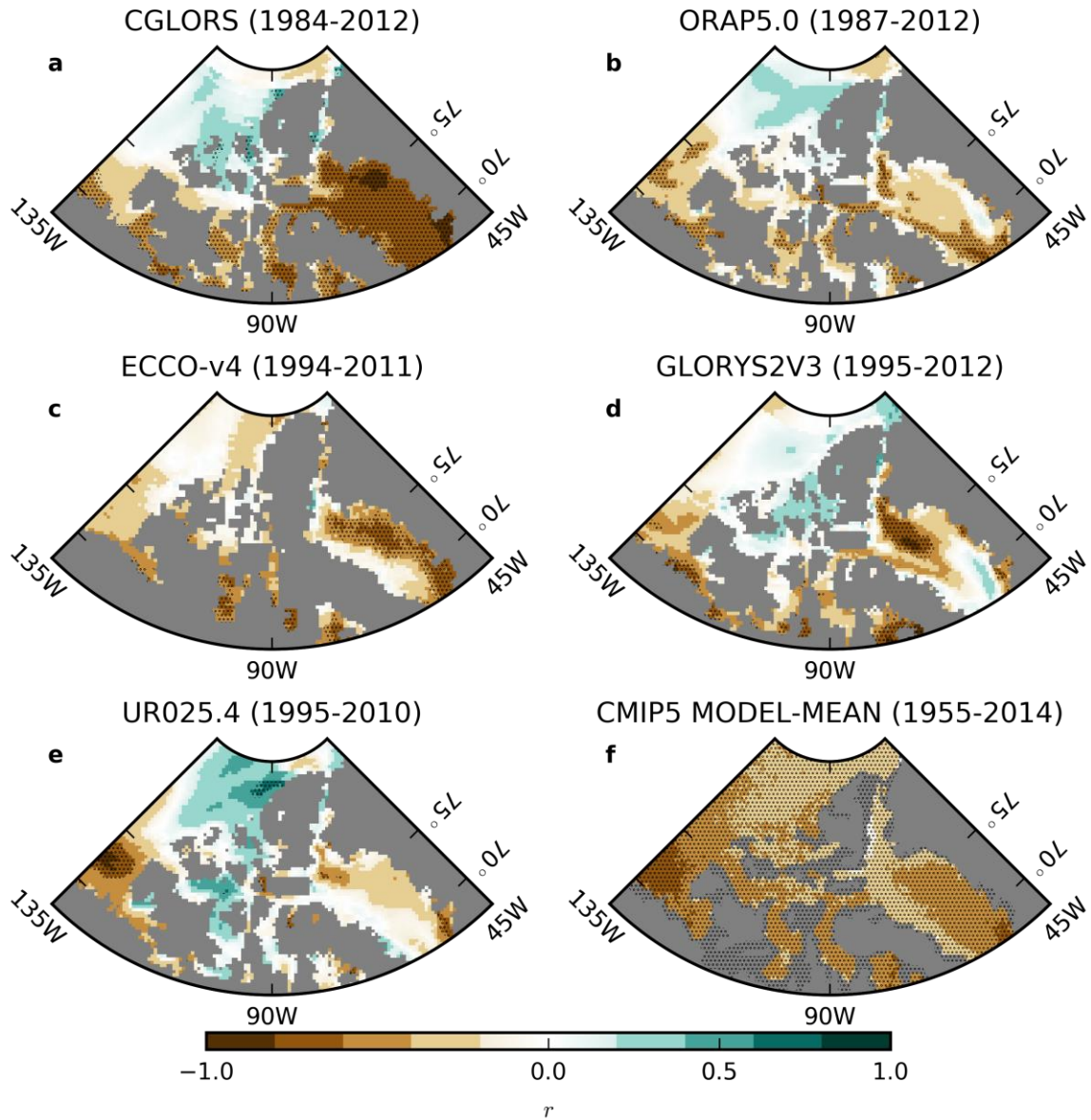


812
 813 Figure 11. Comparison of PIOMAS ice thickness with ice thickness observations from
 814 Environment Canada's ice thickness monitoring sites at Cambridge Bay and Resolute. The data
 815 covers the period 1979-2014.
 816
 817



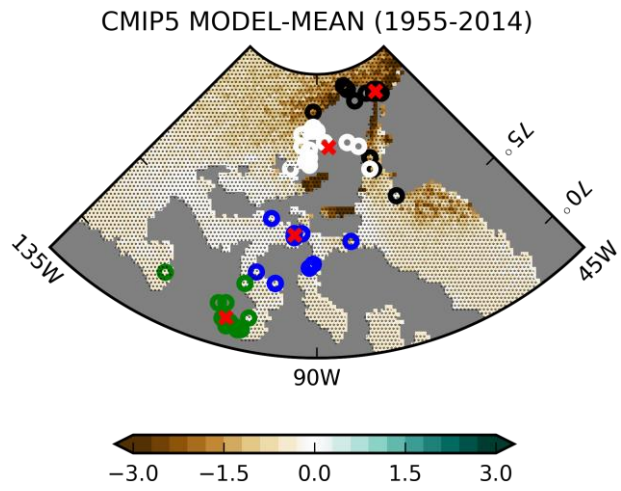
818
 819
 820
 821
 822
 823
 824
 825
 826
 827
 828
 829
 830
 831
 832
 833
 834
 835

Figure 12. **a-e**: Maximum sea ice thickness trends in ORA-IP simulations. **f**: Same for CMIP5 MODEL-MEAN. From South to North, o's indicate Cambridge Bay (green), Resolute (blue), Eureka (white) and Alert (black) and x's indicate the corresponding measurement stations. In f, one o per model is shown." The stippling indicates p-values less than 0.05, corrected using the False Discovery Rate (FDR) method with a global pFDR-values less than 0.10 [Wilks, 2006]. The colorbar is linear from -10 cm dec⁻¹ to 10 cm dec⁻¹ and symmetric logarithmic beyond these values.



836
 837
 838
 839
 840
 841
 842
 843
 844
 845
 846
 847
 848
 849
 850

Figure 13. **a-c**: Pearson correlation of detrended maximum sea ice thickness in ORA-IP with detrended ONDJFMAM ERA-INTERIM 2m temperature. **f**: Same but for CMIP5 MODEL-MEAN. The stippling indicates p-values less than 0.05, corrected using the False Discovery Rate (FDR) method with a global pFDR-values less than 0.10 [Wilks, 2006].



851
852

853 Figure 14. Same as Figure 12f but for snow depth trends (ONDFJMM).